Effect of Mo substitution in the $n=3$ Ruddlesden-Popper compound $Ca_4Mn_3O_{10}$

W. J. Lu, Y. P. Sun,* R. Ang, X. B. Zhu, and W. H. Song

Key Laboratory of Materials Physics, Institute of Solid State Physics, Chinese Academy of Sciences, Hefei, People's Republic of China and Hefei High Magnetic Field Laboratory, Chinese Academy of Sciences, Hefei 230031, People's Republic of China

(Received 19 June 2006; revised manuscript received 8 November 2006; published 10 January 2007)

The effect of Mo doping on the structural, magnetic, electrical, and thermal transport properties of $Ca_4Mn_{3-x}Mo_xO_{10}$ ($0 \leqslant x \leqslant 0.3$) compounds has been investigated. Our study indicates that $Ca_4Mn_3O_{10}$ exhibits a weak ferromagnetism below $T_N=115$ K, which is due to the canting of antiferromagnetic sublattices. The slight Mo doping at Mn sites (for $x=0.03$, 0.06, and 0.1) induces ferromagnetic clusters. The induced ferromagnetism may be ascribed to the double-exchange (DE) interaction between Mn^{4+} and Mn^{3+} ions. For the $x=0.2$ and 0.3 samples, experimental results show that a cluster-glass state dominates at low temperatures due to the competition between the ferromagnetic DE and the antiferromagnetic superexchange interactions. The small polaron hopping and variable range hopping mechanisms have been used to explain the conduction behavior of these samples. Under 7 T field and at 50 K, the maximum magnetoresistance value 45% is observed in the $x=0.1$ sample. The observed negative thermopower S values indicate that the carriers present in all the samples are electrons. Furthermore, the thermal conductivity κ measurement results show the enhanced Jahn-Teller distortions of MnO_6 octahedra and quenched structural disorder due to Mo doping.

DOI: 10.1103/PhysRevB.75.014414 PACS number(s): 75.47.Lx, 64.75.+g, 75.47.Gk

I. INTRODUCTION

Manganites with perovskite structure have been a focus of recent investigation since studies of the colossal magnetoresistance (CMR) effect in the early 1990s.[1–3] The class of perovskite manganites can be regarded as the $n=\infty$ member of a general family of compounds $(R,A)_{n+1}Mn_nO_{3n+1}$, known as Ruddlesden-Popper (RP) phases.[4] The RP phases provide an invaluable experimental model to study the influence of dimensionality on the CMR effect.[5] For general n, the RP phases consist of n layers of perovskite blocks alternating with single $(R,A)O$ rock-salt layer. The introduction of the rock-salt layer increases the interlayer space of the MnO_2 block sheets, thus causing a decrease in the value of the exchange constant in that direction. This produces an anisotropic reduction in the $3d$ bandwidth and hence modifies the magnetic and transport properties of these systems to some extent which depends on the value of n.[6]

The CMR effect found in perovskite manganites is also exhibited by $n=1$ and 2 members of the RP family.[5,7,8] Manganese mixed valence is accepted to play a fundamental role in the CMR behavior of these compounds since the simultaneous appearance of ferromagnetism and enhanced electrical conductivity is explained by the double-exchange (DE) interaction between Mn^{3+} and Mn^{4+} ions.[9] The control of manganese mixed valence can be achieved by the substitution of R and A, e.g., $La_{1-x}Ca_xMnO_3$ and $La_{2-2x}Sr_{1+2x}Mn_2O_7$ for $0.2 < x < 0.5$, extensively investigated in the literature.[3,5,7] The substitution of manganese ions by a different valence cation is another possible way of changing the mixed valence ratio. For instance, Raveau *et al.* reported that the pentavalent and hexavalent d^0 elements (Nb, Ta, W, Mo) substitution at Mn site of $CaMnO_3$ can induce ferromagnetism and CMR.[10] Up to now, few papers have been published on $n=3$ member of the RP series.[11–15] This is mainly due to the difficulty in producing mixed Mn^{3+}/Mn^{4+} materials by chemical substitution, which makes the system a poor candidate for showing CMR through the conventional DE mechanism. Attempts have been made to dope $Ca_4Mn_3O_{10}$ with La^{3+} in order to induce mixed valence, but only small doping levels have been so far reported in bulk samples,[11,12] for values of 0.01 and 0.1. Yu *et al.*[13,14] have shown that the reason for this rather low doping levels could be the instability of the structure of the undoped $Ca_4Mn_3O_{10}$ under the internal chemical pressure originating from the difference in ionic radii between Ca^{2+} and La^{3+}.

Our present investigation is based on the idea that a partial substitution of Mo^{6+} for Mn^{4+} in $Ca_4Mn_3O_{10}$ should induce electron doping, i.e., Mn^{3+} species in the Mn^{4+} matrix, and consequent DE interaction. Considering the high valence state (6+) of doping Mo, one can expect that the substitution of a small content of Mo for Mn should induce a large change in the Mn^{4+}/Mn^{3+} ions ratio. In this work we report the structural, magnetic, electrical, and thermal transport properties of the $Ca_4Mn_{3-x}Mo_xO_{10}$ ($0 \leqslant x \leqslant 0.3$) compounds. The doping with Mo^{6+}, established by x-ray photoelectron spectroscopy (XPS) measurements, introduces electrons in the system, which is consistent with the observed negative thermopower values. The induced ferromagnetism and consequent CMR are observed for the Mo-doped samples due to the ferromagnetic (FM) DE interaction between Mn^{4+} and Mn^{3+} ions. The thermal conductivity measurement results have been discussed in terms of the unusually large distortions of the MnO_6 octahedra and enhanced structural disorder with increase of doping level.

II. EXPERIMENTAL

Polycrystalline $Ca_4Mn_{3-x}Mo_xO_{10}$ ($x=0$, 0.03, 0.06, 0.1, 0.2, and 0.3) samples were synthesized by the standard solid-state reaction. Stoichiometric precursor powders $CaCO_3$, MnO_2 and MoO_3 were mixed and ground, then fired in air several times at 950 °C, 1100 °C, and 1200 °C for 24 h with intermediate grinding. After the final grinding, the pow-

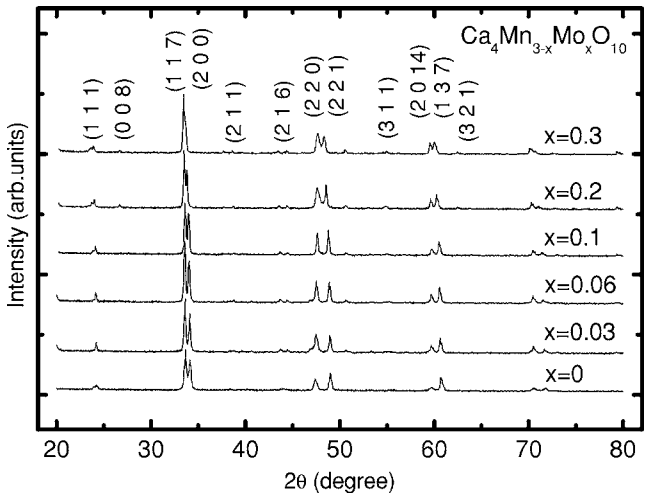

FIG. 1. XRD patterns for $Ca_4Mn_{3-x}Mo_xO_{10}$ with $x=0$, 0.03, 0.06, 0.1, 0.2, and 0.3.

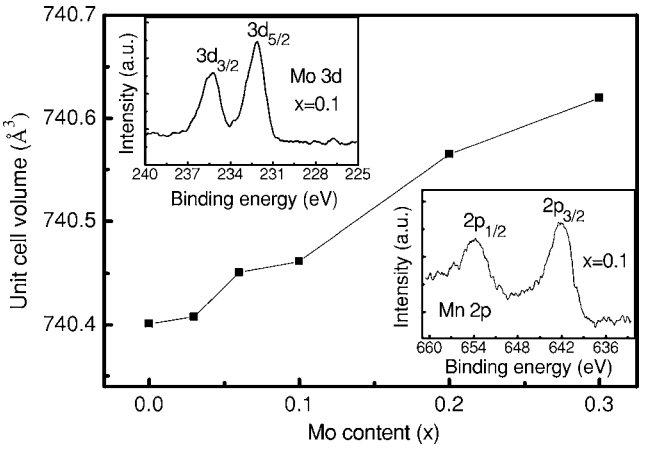

FIG. 2. Unit cell volume, V, as a function of Mo doping content x. The inset shows XPS spectra of Mo $3d$ and Mn $2p$ regions for the selected $x=0.1$ sample.

der was pressed into small pellets, sintered in air at 1250 °C for 24 h and slow cooled to room temperature.

The room temperature x-ray diffraction (XRD) measurement was taken by Philips X'pert PRO x-ray diffractometer with Cu $K\alpha$ radiation. The structural parameters were obtained by fitting the experimental data of XRD using the standard Rietveld technique. XPS measurements were performed using VG Scientific ESCALAB MKII spectrometer, with Mg $K\alpha$ x-ray as the excitation source. The magnetic measurements were carried out with a Quantum Design superconducting quantum interference device (SQUID) MPMS system. The resistivity ρ, thermopower S, and thermal conductivity κ were performed on a Quantum Design physical property measurements system (PPMS).

III. RESULTS AND DISCUSSION

The room temperature XRD patterns of $Ca_4Mn_{3-x}Mo_xO_{10}$ ($x=0$, 0.03, 0.06, 0.1, 0.2, and 0.3) are shown in Fig. 1. The Rietveld refinements of the XRD patterns show that all samples are single phase with no detectable secondary phases. The XRD patterns can be indexed as the RP phase with orthorhombic symmetry (space group *Pbca*). For the undoped sample, we obtained $a=5.2519(4)$ Å, $b=5.2635(4)$ Å, and $c=26.7840(9)$ Å, close to the data reported in a previous paper.[15] For the doped samples, the cell parameters are expected to vary with Mo doping content x. If one takes into account the possible Mo^{6+} oxidation state in the doped samples, the molybdenum for manganese substitution will lead some reduction of Mn^{4+} to Mn^{3+}. As shown in Fig. 2, the unit-cell volume monotonously increases with increase of x, which is consistent with the increase of induced Mn^{3+} (0.645 Å) whose ion radius is larger than that of Mn^{4+} (0.53 Å). In fact, Pi *et al.*[16] have suggested that the oxidation state of Mo in $CaMn_{1-x}Mo_xO_3$ perovskites should be Mo^{6+}. In order to establish the real valence states of Mo and Mn ions in our doped samples, we carried XPS measurements on Mo $3d$ and Mn $2p$ regions. The inset of Fig. 2 shows the XPS spectra of Mo $3d_{5/2}$ and $3d_{3/2}$ for the selected $x=0.1$ sample. From this figure one can find that the binding energies of Mo $3d_{5/2}$ and $3d_{3/2}$ are 232.1 and 235.3 eV respectively, with a splitting of 3.2 eV. These observed binding energies are related with Mo^{6+}.[17] Thus, the valence of Mo in our doped samples can be established as 6+, which is not surprising since the most stable valence of Mo in air is 6+ (d^0 configuration). The peak of Mn $2p_{3/2}$ is broad and the center locates at binding energy of 642.0 eV (see the inset of Fig. 2). When manganese has a 4+ (i.e., MnO_2) or 3+ (i.e., MnOOH), the peak of Mn $2p_{3/2}$ is expected at 642.2 eV or 641.5 eV. Therefore, the manganese in our studies presents an intermediate valence (between 4+ and 3+). Then the induced ferromagnetism and consequent CMR can be expected due to the DE interaction between Mn^{4+} and Mn^{3+} ions.

Figure 3 shows the temperature dependence of magnetic susceptibility, $\chi(T)$, measured under an applied field of 0.1 T. For the undoped $Ca_4Mn_3O_{10}$, the zero-field-cooling (ZFC) curve shows a cusp at $T_N \sim 115$ K [see Fig. 3(a)], indicating a typical antiferromagnetic (AFM) behavior. This result is in qualitative agreement with neutron-scattering studies.[15] The field-cooling (FC) curve shows a sharp increase at a temperature of ~115 K, which is associated with a weak ferromagnetism (WFM) in $Ca_4Mn_3O_{10}$.[6,15] Magnetization as a function of applied field also evidences a small FM component (Fig. 4). The WFM as an intrinsic property of $Ca_4Mn_3O_{10}$ is most probably due to the canting of AFM sublattices due to an antisymmetric Dzyaloshinskii-Moriya (DM) term in the exchange Hamiltonian arising from the orthorhombic distortion of the crystal structure.[6] The WFM is hidden in zero field due to the AFM exchange interaction but an applied magnetic field induces a spin-flop transition into a phase with a net magnetization. Interestingly, the drop in FC magnetization is observed below 35 K. This drop is evidence for a more complex behavior than expected for a conventional weak ferromagnet. Thermoremanent magnetization (TRM) measurements[6] have indicated that the low-temperature complex behavior could be associated with a spin-glass-like phase due to the disorder of the WFM moment in each MnO_2 plane.

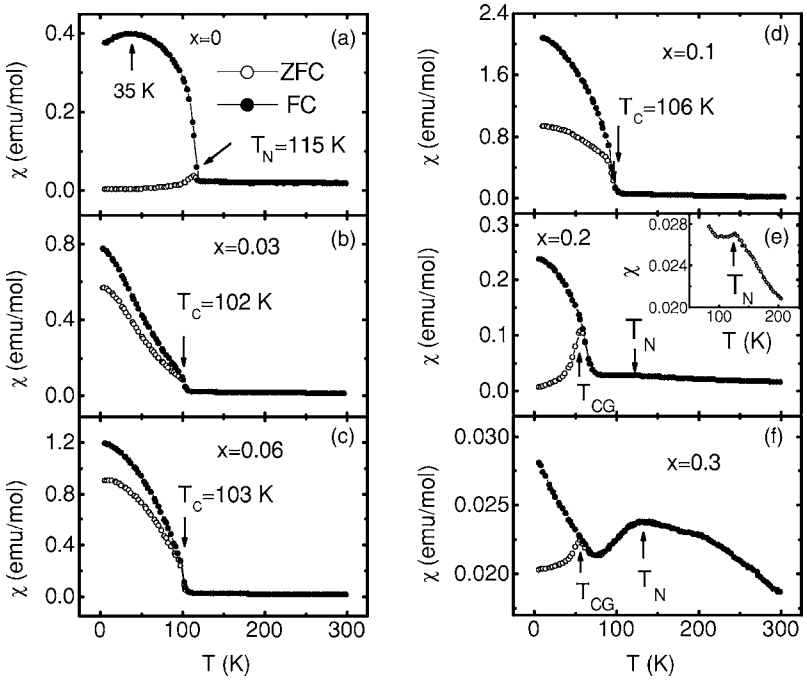

FIG. 3. Magnetic susceptibility, χ, as a function of temperature under zero field cooling (ZFC) and field cooling (FC) at $H=0.1$ T. T_N, the antiferromagnetic transition temperature. T_C, the ferromagnetic transition temperature. T_{CG}, the cluster-glass state transition temperature.

The $\chi(T)$ curves of the $x=0.03$, 0.06, and 0.1 samples are quite different from that of the undoped sample. As shown in Fig. 3(b)–3(d), the shape of the ZFC and FC curves displays ferromagnetism-like behavior, with a transition temperature $T_C \sim 105$ K. The magnetic susceptibility and T_C value increase with the doping level x. The observed ferromagnetism in the lightly doped samples should originate from the DE interaction between Mn^{4+} and Mn^{3+} induced by the Mo^{6+} doping at Mn sites. The doped electrons remain localized on single Mn sites leading to isolated Mn^{3+} ions that coexist with the majority Mn^{4+} sites. The DE coupling to the neighboring Mn^{4+} ions distorts the magnetic environment locally creating a FM cloud around itself. The small variation of T_C results from a competition mechanism. On the one hand, the DE interaction should be enhanced due to the increasing Mn^{3+} content with the doping level x. On the other hand, the structure distortion is enhanced due to the Jahn-Teller (JT) effect of Mn^{3+} ions. As a result, the Mn-O-Mn bond angle decreases and the DE interaction should be weakened. Due to the above two competitive ways, T_C only has a small variation. Additionally, there exist distinct differences between ZFC and FC curves just below T_C and the susceptibility cannot reach saturation at low temperatures, which are reminiscent of an inhomogeneous ferromagnetism.[18] Such magnetic inhomogeneity was previously observed in Mn-site doped perovskite $CaMnO_3$, e.g., $CaMn_{1-x}Ru_xO_3$ and $CaMn_{1-x}Mo_xO_3$.[16] Considering the induced DE coupling by Mo substitution, a long-range FM ordering can be expected for the doped samples with high doping level $x=0.2$ and 0.3. However, that is not the case. Figures 3(e) and 3(f) show that the AFM state appears at a transition temperature T_N ($T_N=120$ and 135 K for $x=0.2$ and 0.3, respectively). The observed AFM ordering can be related to the Mn^{3+}/Mn^{3+} superexchange interaction, which cannot be ignored as the Mn^{3+} content increases with doping level. In the absence of long-range FM ordering, the irreversibility between ZFC and FC curves at low temperatures indicates a glass-like transition resulting from the AFM ordering and the short-range FM interactions. The low-temperature state is cluster-glass rather than spin-glass phase, since the induced DE FM clusters are embedded in an AFM matrix as discussed above. The competing phases, AFM and FM, can result in the existence of inhomogeneous state and consequent phase separation.[19] This picture is similar to that in $Ca_{1-x}La_xMnO_3$ and $Ca_{1.92}La_{0.08}MnO_4$ reported in the literature.[20,21]

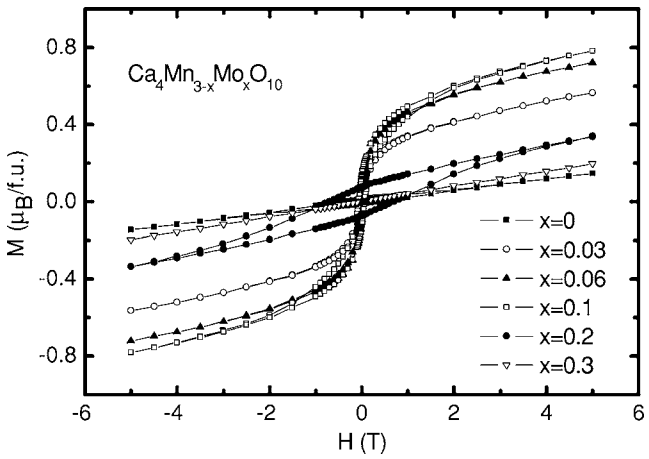

FIG. 4. The M-H loops at 10 K for $Ca_4Mn_{3-x}Mo_xO_{10}$ ($0 \leqslant x \leqslant 0.3$).

The M-H loops of all the samples were measured at the temperature of 10 K. The experimental results are shown in Fig. 4. For the undoped $Ca_4Mn_3O_{10}$, M increases almost linearly with H and a very small hysteresis is observed, indicating an AFM phase with WFM. For the $x=0.03$, 0.06, and 0.1 samples, M rises sharply with the increase of H at low fields and does not saturate even at 5 T, which reveals a superposition of both FM and AFM components. With fur-

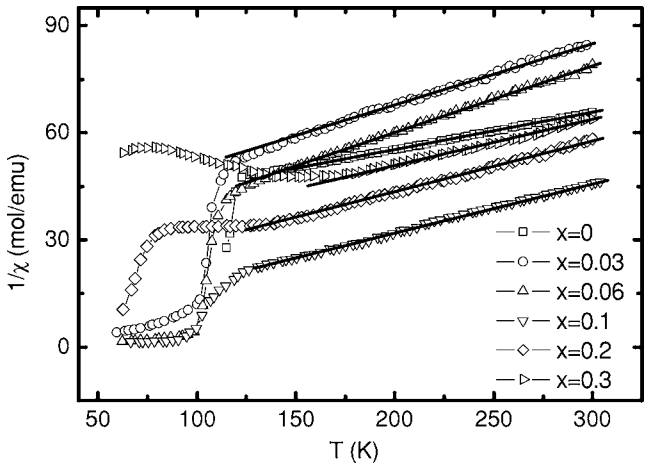

FIG. 5. Inverse susceptibility as a function of temperature. The solid lines represent the fitting data according to the Curie-Weiss law.

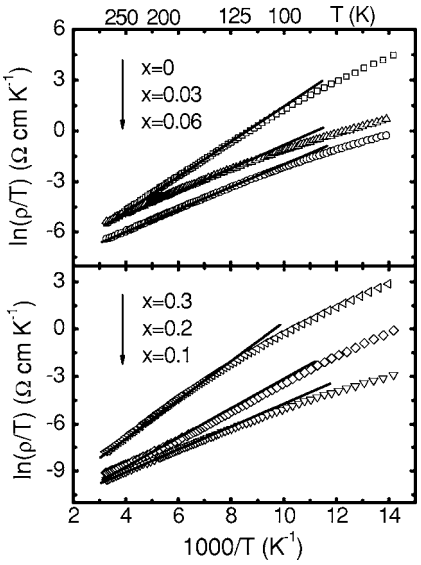

FIG. 6. The $\ln(\rho/T)$ as a function of $1000/T$. The solid lines are the fitting data according to the small polaron hopping model.

ther increasing the doping level x (for 0.2 and 0.3), the magnetization decreases due to the enhanced Mn^{3+}/Mn^{3+} AFM interaction. Interestingly, especially for the $x=0.2$ sample, the magnetic hysteresis appears even at a high field of 4.5 T and the coercive force H_C is fairly large. Such a large H_C is due to the large blocking of the domain wall motion in the magnetic inhomogeneity state of this sample.

In order to study the magnetic interaction further, we fitted the experimental data in paramagnetic (PM) region according to the Curie-Weiss law, $\chi=C/(T-\theta_P)$, where C is the Curie constant and θ_P is Weiss temperature. Figure 5 shows the temperature dependence of the inverse susceptibility, $1/\chi$, and the fitting curves. For all samples, the experimental data in PM region can be well fitted by the Curie-Weiss law. The fitted values of θ_P are −539, −177, −115, −28, −94, and −223 K for $x=0$, 0.03, 0.06, 0.1, 0.2, and 0.3 respectively. For $x=0$, the deduced θ_P value of −539 K is anomalously high when compared with T_N, consistent with the reported results in the literatures.[6,22] For all doped samples, the θ_P values are negative, which indicates the existence of AFM interactions. With increasing x, the absolute value of θ_P originally decreases and then increases, which reaches the minimum as $x=0.1$. The variation of θ_P could be associated with the competition between the AFM and FM interactions. As $x\leqslant 0.1$, the induced DE interaction weakens the AFM interaction between Mn^{4+} ions, resulting in the decrease of $|\theta_P|$. As $x>0.1$, the AFM interaction between Mn^{3+} ions is enhanced, resulting in the increase of $|\theta_P|$. The effective magnetic moment μ_{eff} values obtained on the basis of Curie-Weiss law are 4.38, 4.42, 4.53, 5.20, 5.11, and $5.03\mu_B$ per manganese ion for $x=0$, 0.03, 0.06, 0.1, 0.2, and 0.3 respectively. Although the negative θ_P values strongly support the existence of strong AFM interactions, the observed μ_{eff} values are much larger than the calculated values using the spin-only moment of the free Mn ions ($3.87\mu_B$ for Mn^{4+} and $4.90\mu_B$ for Mn^{3+}). Such large μ_{eff} values indicate that there should exist some short-range magnetic interaction in high-temperature PM region. The existence of the probably strongest short-range magnetic interaction in the $x=0.1$ sample could account for the maximum μ_{eff} value. As $x>0.1$, the short-range magnetic interaction is gradually weakened, thus the μ_{eff} value decreases with increasing x.

The zero-field resistivity of our samples is plotted versus inverse temperature in Fig. 6. All the samples show semiconducting behavior over the whole measuring temperature range. By comparing with the resistivity data of perovskite $CaMn_{1-x}Mo_xO_3$,[16] the ρ of $Ca_4Mn_{3-x}Mo_xO_{10}$ is obviously higher. This is attributed to the difference in structures of these two systems. It is known that $CaMnO_3$ has the perovskite structure characterized by a three-dimensional array of corner-sharing MnO_6 octahedra. However, in $Ca_4Mn_3O_{10}$, every three $CaMnO_3$ perovskite layers is separated by a rock-salt layer. Therefore, the larger ρ of $Ca_4Mn_{3-x}Mo_xO_{10}$ is reasonably associated with the introduction of the insulating rock-salt type CaO layers between the perovskite blocks. For the $x\leqslant 0.1$ samples, the resistivity decreases with increasing Mo doping level, consistent with the increase of e_g electrons and induced ferromagnetism as discussed above. However, with increasing x further (for $x>0.1$), the resistivity increases with x. This should be ascribed to the enhanced lattice distortions due to the JT effect of Mn^{3+} and the induced disorder due to Mo doping at Mn sites.

The solid lines in Fig. 6 correspond to the fit of the experimental data to a small polaron model, in which case the resistivity can be expressed by the formula:[23]

$$\rho = \rho_0 T \exp\left(\frac{E_\alpha}{k_B T}\right). \tag{1}$$

This formula predicts a linear relation between $\ln(\rho/T)$ and $1/T$, and E_α/k_B is the slope of the straight line. For all the samples, as shown in Fig. 6, the resistivity can be well fitted using the small polaron model for $T>T_N$ (T_C), with activation energies of 86.3, 75.4, 60.5, 55.9, 66.2, and 107.6 meV for $x=0$, 0.03, 0.06, 0.1, 0.2, and 0.3, respectively. For $x=0.2$ and 0.3 samples, the E_α value unusually increases, which is attributed to the increase of polaron binding energy

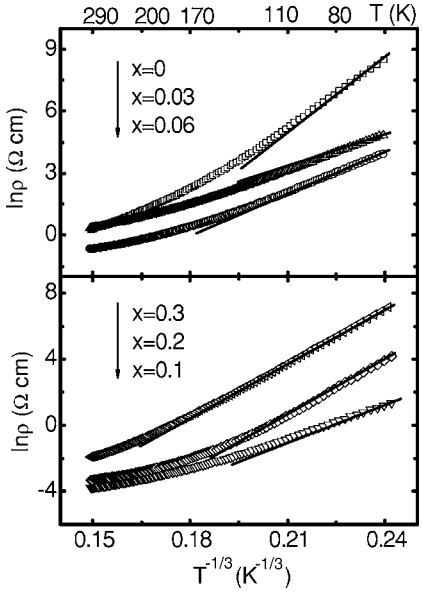

FIG. 7. ln ρ as a function of $T^{-1/3}$. The solid lines represent the fitting data according to the 2D VRH model described in the text.

due to the enhanced JT distortion. One can find that there are more marked deviations at low temperatures, indicating a change in the conduction mechanism. In fact, below T_N (T_C), the resistivity is best described in terms of 2D Mott's variable range hopping (VRH) model:[23]

$$\rho = \rho_0 \exp\left[\left(\frac{T_0}{T}\right)^{1/3}\right]. \tag{2}$$

The fitting results are shown in Fig. 7. Especially for $x=0.2$ and 0.3 samples, the fit to the VRH model is reasonably good, due to the induced large disorder effect on the conduction. The results show that the fitting parameter $T_0=2.3\times10^6$ K for $x=0$ and $T_0=1.2\times10^7$ K for the highest doping level $x=0.3$. According to Mott's VRH theory the parameter T_0 is inversely proportional to the localization length of the carriers. So a large value of T_0 implies the existence of a great disorder. Therefore, for our samples, the increase of T_0 value with x indicates the enhanced disorder due to the Mo doping.

Considering the induced ferromagnetism in our doped samples, these samples are expected to show a CMR behavior especially at low temperatures. We performed the resistivity measurements under an applied magnetic field of 7 T for all the samples. The temperature dependence of the negative MR ratio $-\Delta\rho/\rho(0)$ is shown in Fig. 8. The MR ratio is defined as $\Delta\rho/\rho(0)=[\rho(H)-\rho(0)]/\rho(0)$, where $\rho(0)$ is the resistivity at zero field and $\rho(H)$ is the resistivity at the applied field of 7 T. As shown in Fig. 8, the MR values of the doped samples are much larger than that of the undoped sample, especially for the $x=0.03$, 0.06, and 0.1 samples, and the maximum MR value reaches 45% at 50 K for $x=0.1$ sample with the maximum T_C (see Fig. 3). The observed large MR effect should be related to the existence of ferromagnetism at low temperatures. A spin-dependent mechanism of MR could, in principle, have an intrinsic as well as

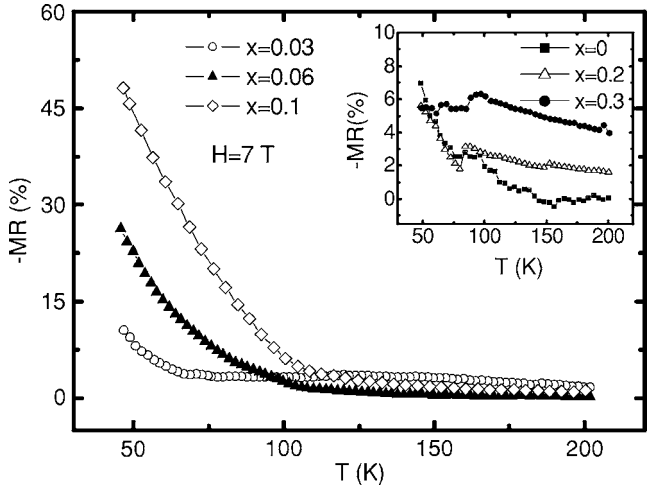

FIG. 8. Temperature dependence of negative magnetoresistance (MR) ratio under an applied magnetic field of 7 T.

an extrinsic origin. The former is due to the reduction in spin disorder caused by the increasing magnetic polarization of the sample as the applied field rises. The latter is associated with spin-polarized tunneling between FM grains (i.e., an extrinsic effect).[24] For the $x=0$, 0.2, and 0.3 samples, the most likely mechanism of the MR in our samples is spin-dependent scattering, considering the existence of only weak ferromagnetism in these samples. In contrast, for $x=0.03$, 0.06, and 0.1 samples, the MR is significant only in the presence of magnetic order below T_C, indicating MR mechanism may be dominated by spin-polarized tunneling. Anyway, further study is necessary to clarify the certain mechanism of MR in our samples.

The temperature dependence of the thermopower, $S(T)$, is presented in Fig. 9. As expected, S values are negative over the whole temperature range measured, indicating that the majority carriers in $Ca_4Mn_{3-x}Mo_xO_{10}$ ($0\leqslant x\leqslant 0.3$) are electrons. The values of S of all samples increase on cooling are typical of semiconducting behavior, in agreement with resistivity results above. Moreover, the absolute values of S decrease with increasing the Mo content, consistent with the

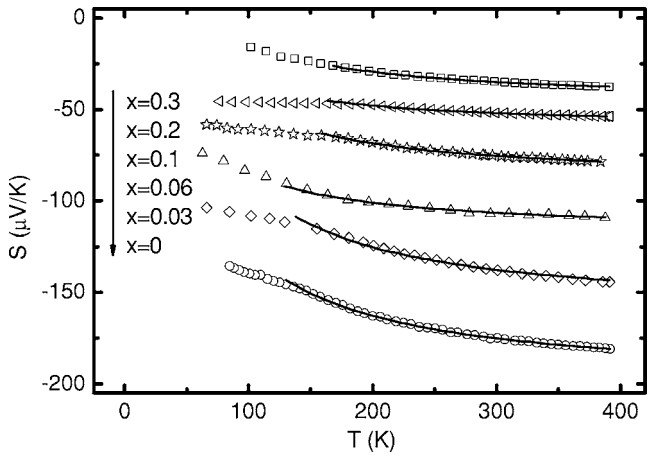

FIG. 9. Temperature dependence of thermopower S. The solid lines are fitting curves using the small polaron hopping model.

increase of carriers due to Mo doping. For the undoped $Ca_4Mn_3O_{10}$, the large magnitude ($|S|>180\ \mu V\ K^{-1}$ above 300 K) and almost T independence at high temperatures show the advantage for thermoelectric application. In the temperature range 150–400 K, for all the sample, the temperature dependence of S can be fitted to small polaron hopping theory, according to which S can be expressed as[25]

$$S = -\frac{k_B}{e}\left(\frac{E_S}{k_B T} + A\right), \tag{3}$$

where E_S is the thermopower activation energy and A represents the contribution to S of electrons distributed in states above the conduction band edge. As shown in Fig. 9, the fit is not satisfied exactly over the stated range, however it is clearly the best fit compared to other alternative models. The activation energies E_S obtained from the thermopower data are 17.2, 15.1, 14.3, 13.9, 12.1, and 13.4 meV for $x=0$, 0.03, 0.06, 0.1, 0.2, and 0.3, respectively. The deduced E_S values are significantly below the values of the activation energies E_α derived from the resistivity measurements, which is characteristic of small polaron hopping transport.[26] In this instance, E_α is normally assumed to be the sum of two relevant parts: $E_\alpha = W_H + E_S$. Here W_H is the activation energy corresponding to the minimum energy to produce the equivalency of the two neighboring sites involved in the polaron hopping, and is equal to one-half of the polaron binding energy. For our samples, the large difference between E_α and E_S signifies that conventional band transport does not occur, but rather is the hallmark of small polaron hopping wherein the transport is dominated by temperature dependent mobility effects. Furthermore, one can notice that the E_S value for $x=0.3$ is larger than that for $x=0.2$. As discussed above, transport occurs via thermally activated hopping of small polaron, in which case E_S is the energy difference between identical lattice distortions with and without the carrier, in other words, E_S is the energy required to generate the carrier. Thus, the increase of polaron band gap could be one main reason for the increase of E_S value. In the low-temperature range of $T<150$ K, S cannot be fitted by small polaron hopping model, which may indicate a change in the transport process. However, the certain mechanism cannot be deduced from only several reliable data points, because we cannot measure S values at low temperatures due to the very high resistivity of all the samples.

Figure 10 shows the thermal conductivity κ of $Ca_4Mn_{3-x}Mo_xO_{10}$ ($0 \leqslant x \leqslant 0.3$). In general, κ can be expressed by the sum of a lattice component κ_l and an electronic component κ_e as $\kappa = \kappa_l + \kappa_e$. Usually, κ_e can be estimated by the Wiedemann-Franz (W-F) law, which relates κ_e to the electrical conductivity according to $\kappa_e = L_0 \sigma T$. Here, $L_0 = 2.45 \times 10^{-8}\ W\ \Omega\ K^{-2}$ denotes the Sommerfeld value of the Lorenz number. From the measured values of ρ, we estimate that κ_e is less than 5% of κ for all samples. Thus, $\kappa(T)$ is dominated by phonons and κ_e is negligible in this case. We concentrate first on the undoped sample. As shown in Fig. 10, the κ rapidly increases with temperature at low temperatures and reaches a maximum value at about 70 K. In the temperature range 70–200 K, κ decreases with temperature. However, above 200 K κ increases slowly with increasing

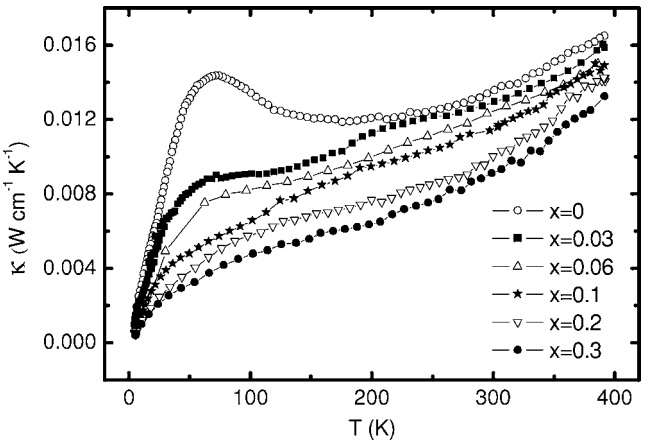

FIG. 10. Temperature dependence of thermal conductivity κ for all samples.

temperature, which is anomalous for usual phononic heat transport. A qualitative understanding of the phononic heat transport is obtained from the relation $k \propto cvl$, where c, v, and l denote the specific heat, the sound velocity, and the mean free path of the phonons, respectively. At low temperatures, l is determined by lattice imperfections, and the temperature dependence of κ follows that of the specific heat, i.e., $\kappa \propto T^3$ for $T \to 0$ K. At intermediate temperatures a maximum of κ occurs, when phonon-phonon Umklapp scattering becomes important and leads to a decrease of l with increasing temperature. At high temperatures Umklapp scattering is proportional to the number of phonons which is proportional to temperature, i.e., $l \propto 1/T$ and κ follows a $1/T$ dependence. Above 200 K, the observed unusual temperature dependence ($d\kappa/dT>0$), the behavior of an amorphous solid, indicates that an unusual, additional scattering mechanism is active. In fact, the positive $d\kappa/dT$ is usually observed in manganites. Unlike amorphous solids, $d\kappa/dT>0$, here is not related to quenched structural disorder but rather to unusually large dynamic lattice distortions.[27,28] For the undoped sample, as pointed by Battle *et al.*,[15] very small content of Mn^{3+} may exist because the oxygen stoichiometry is not perfect. Thus the local distortions of the MnO_6 octahedra due to the JT effect can be expected to account for the anomalous high-temperature κ behavior. For the doped samples, the values of κ decrease with increasing Mo doping content x, and the maximum κ at 70 K is suppressed. This could arise from the enhanced lattice distortions and the induced disorder due to Mo doping at Mn sites.

IV. CONCLUSIONS

In summary, Mo doped $Ca_4Mn_{3-x}Mo_xO_{10}$ ($0 \leqslant x \leqslant 0.3$) system was synthesized and the structural, magnetic, electrical, and thermal transport properties have been systematically investigated. The experimental results show that Mo doping induces FM clusters in the AFM matrix due to DE interaction between Mn^{4+} and Mn^{3+} ions. Accordingly, the large MR effect has been observed in the $x=0.03$, 0.06, and 0.1 samples especially at low temperatures. The electrical

conduction mechanisms can be well described as small polaron hopping and variable range hopping at high temperatures and low temperatures, respectively. The thermopower S values are negative over the whole temperature range measured, indicating electronic doping in $Ca_4Mn_{3-x}Mo_xO_{10}$ ($0 \leqslant x \leqslant 0.3$). The thermal conductivity κ measurements show the unusually large dynamic JT distortion of MnO_6 octahedra and the induced disorder due to Mo doping at Mn sites.

ACKNOWLEDGMENTS

The authors want to thank W. B. Wu at University of Science and Technology of China for his help in the measurements. This work is supported by the National Key Basic Research under Contract No. 001CB610604, the National Nature Science Foundation of China under Contract Nos. 10474100 and 50672099, and Director's Fund of Hefei Institutes of Physical Science, Chinese Academy of Sciences.

*Corresponding author. Email address: ypsun@issp.ac.cn

[1] R. M. Kusters, J. Singleton, D. A. Keen, R. McGreevy, and W. Hayes, Physica B **155**, 362 (1989).
[2] R. von Helmolt, J. Wecker, B. Holzapfel, L. Schultz, and K. Samwer, Phys. Rev. Lett. **71**, 2331 (1993).
[3] Y. Tokura, *Colossal Magnetoresistance Oxides* (Gordon and Breach, New York, 2000).
[4] S. N. Ruddlesden and P. Popper, Acta Crystallogr. **11**, 541 (1958).
[5] Y. Moritomo, A. Asamitsu, H. Kuwahama, and Y. Tokura, Nature **380**, 141 (1996).
[6] J. Lago, P. D. Battle, and M. J. Rosseinsky, J. Phys.: Condens. Matter **12**, 2505 (2000).
[7] T. Kimura, A. Asamitsu, Y. Tomioka, and Y. Tokura, Phys. Rev. Lett. **79**, 3720 (1997).
[8] A. Maignan, C. Martin, G. Van Tendeloo, M. Hervieu, and B. Raveau, J. Mater. Chem. **8**, 2411 (1998).
[9] C. Zener, Phys. Rev. **82**, 403 (1951).
[10] B. Raveau, Y. M. Zhao, C. Martin, M. Hervieu, and A. Maignan, J. Solid State Chem. **149**, 203 (2000).
[11] N. S. Witte, P. Goodman, F. J. Lincoln, R. H. March, S. J. Kennedy, Appl. Phys. Lett. **72**, 853 (1998).
[12] H. Asano, J. Hayakawa, and M. Matsui, Appl. Phys. Lett. **71**, 844 (1997).
[13] R. C. Yu, S. Y. Li, J. L. Zhu, F. Y. Li, Z. Zhang, C. Q. Jin, and I. G. Voigt-Martin, J. Appl. Phys. **90**, 6302 (2001).
[14] R. C. Yu, G. W. Meng, L. C. Chen, Z. X. Bao, C. X. Liu, J. L. Zhu, F. Y. Li, Z. X. Liu, J. Liu, and C. Q. Jin, J. Appl. Phys. **91**, 6765 (2002).
[15] P. D. Battle, M. A. Green, J. Lago, J. E. Millburn, M. J. Rosseinsky, and J. F. Vente, Chem. Mater. **10**, 658 (1998).
[16] L. Pi, S. Hébert, C. Martin, A. Maignan, and B. Raveau, Phys. Rev. B **67**, 024430 (2003).
[17] M. Probst, M. Vop, R. Denecke, L. Viscido, I. M. Heras, D. Borgmann, and H. P. Steinruck, J. Electron Spectrosc. Relat. Phenom. **114-116**, 539 (2001).
[18] J. A. Mydosh, *Spin Glass: An Experimental Introduction* (Taylor & Francis, London, 1993).
[19] E. Dagotto, T. Hotta, and A. Moreo, Phys. Rep. **344**, 1 (2001).
[20] A. L. Cornelius, B. E. Light, and J. J. Neumeier, Phys. Rev. B **68**, 014403 (2003).
[21] C. Autret, C. Martin, R. Retoux, A. Maignan, B. Raveau, G. André, F. Bourée, and Z. Jirak, J. Magn. Magn. Mater. **284**, 172 (2004).
[22] I. D. Fawcett, J. E. Sunstrom, M. Greenblatt, M. Croft, K. V. Ramanujachary, Chem. Mater. **10**, 3643 (1998).
[23] N. F. Mott and E. A. Davis, *Electronic Processes in Non-Crystalline Materials* (Clarendon Press, Oxford, 1979).
[24] H. Y. Hwang, S.-W. Cheong, N. P. Ong, and B. Batlogg, Phys. Rev. Lett. **77**, 2041 (1996).
[25] M. M. Savosta, J. Hejtmánek, Z. Jirák, M. Maryško, P. Novák, Y. Tomioka, and Y. Tokura, Phys. Rev. B **61**, 6896 (2000).
[26] J. Lago, P. D. Battle, M. J. Rosseinsky, A. I. Coldea, and J. Singleton, J. Phys.: Condens. Matter **15**, 6817 (2003).
[27] D. W. Visser, A. P. Ramirez, and M. A. Subramanian, Phys. Rev. Lett. **78**, 3947 (1997).
[28] J.-S. Zhou and J. B. Goodenough, Phys. Rev. B **64**, 024421 (2001).